Acta Oceanol. Sin., 2017, Vol. 36, No. 9, P. 1–9
DOI: 10.1007/s13131-017-1104-1
http://www.hyxb.org.cn
E-mail: hyxbe@263.net

A dual-period response of the Kuroshio Extension SST to Aleutian Low activity in the winter season

YU Peilong[1], ZHANG Lifeng[1]*, LIU Hu[2], LIU Xing[3], ZHU Juan[3]

[1] College of Meteorology and Oceanography, National University of Defense Technology, Nanjing 211101, China

[2] No.61741 Troops of PLA, Beijing 100025, China

[3] Maritime Environment Project Office, Beijing 100081, China

Received 12 October 2016; accepted 3 February 2017

Abstract

Based on our previous work, the winter sea surface temperature (SST) in the Kuroshio Extension (KE) region showed significant variability over the past century with periods of ~6 a between 1930 and 1950 and ~10 a between 1980 and 2009. How the activity of the Aleutian Low (AL) induces this dual-period variability over the two different timespans is further investigated here. For the ~6 a periodicity during 1930–1950, negative wind stress curl (WSC) anomalies in the central subtropical Pacific associated with an intensified AL generate positive sea surface height (SSH) anomalies. When these wind-induced SSH anomalies propagate westwards to the east of Taiwan, China two years later, positive velocity anomalies appear around the Kuroshio to the east of Taiwan and then the mean advection via this current of velocity anomalies leads to a strengthened KE jet and thus an increase in the KE SST one year later. For the ~10 a periodicity during 1980–2009, a negative North Pacific Oscillation-like dipole takes 2–3 a to develop into a significant positive North Pacific Oscillation-like dipole, and this process corresponds to the northward shift of the AL. Negative WSC anomalies associated with this AL activity in the central North Pacific are able to induce the positive SSH anomalies. These oceanic signals then propagate westward into the KE region after 2–3 a, favoring a northward shift of the KE jet, thus leading to the warming of the KE SST. The feedbacks of the KE SST anomaly on the AL forcing are both negative for these two periodicities. These results suggest that the dual-period KE SST variability can be generated by the two-way KE-SST-AL coupling.

Key words: sea surface temperature, Kuroshio Extension, Aleutian Low activity, dual-period variability

Citation: Yu Peilong, Zhang Lifeng, Liu Hu, Liu Xing, Zhu Juan. 2017. A dual-period response of the Kuroshio Extension SST to Aleutian Low activity in the winter season. Acta Oceanologica Sinica, 36(9): 1–9, doi: 10.1007/s13131-017-1104-1

1 Introduction

The Kuroshio Extension (KE) carries the eastward flow of the Kuroshio Current into the open basin of the North Pacific. As a result of the cold and dry continental air overriding the warm water transported poleward by the Kuroshio, the KE lies in the region where the largest ocean-to-atmosphere heat loss occurs during mid-latitude winter (Qiu, 2000; Kelly et al., 2010), which acts as the obvious thermal forcing on the atmosphere. Some research works have pointed out that the sea surface temperature (SST) changes in the KE region are the prime driver of its surface heat flux variations (Tanimoto et al., 2003; Sugimoto and Hanawa, 2011). By affecting heat exchange on the air-sea interface, the KE SST anomaly may have a significant impact on the local and even global climate, and this has been verified by numerous previous studies (e.g., Liu et al., 2007; Frankignoul and Sennéchael, 2007; Wang et al., 2011, 2012). Therefore, the KE SST variability and its underlying mechanism are important issues that require further investigation in the context of predicting North Pacific climate variation.

Previous studies suggested that the KE SST exhibited a dominant variability with a period of ~10 a and this decadal variation was mainly controlled by the wind-induced Rossby waves that were closely related to the KE dynamic state changes (Seager et al., 2001; Kwon and Deser, 2007; Qiu et al., 2007). Specifically, when the wind stress curl (WSC) anomalies in the central North Pacific are positive, enhanced Ekman divergence generates negative local sea surface height (SSH) anomalies. After these oceanic signals propagate westward into the KE region with a delay of a few years, they favor the weakening and southward shift of the KE jet (Qiu, 2003; Qiu and Chen, 2005, 2010; Qiu et al., 2014). These KE dynamic state fluctuations favor a decrease in the geostrophic heat advection, resulting in cooling in the KE region (Qiu, 2000; Vivier et al., 2002). The reverse holds when the WSC anomalies in the central North Pacific are negative. Moreover, the central North Pacific WSC anomalies are predominantly modulated by the variations of Aleutian Low (AL) activity (Ishi and Hanawa, 2005). In this sense, the AL activity changes may have a significant impact on the variation of KE SST variability. Indeed, Sugimoto and Hanawa (2009) verified that the AL north-south shift can induce the ~10 a KE SST variability via the wind-driven Rossby waves.

However, in previous studies, the adopted data had been only available since 1950. The limited length of data may hinder the cognition about the KE SST variability and its linkage with the AL

Foundation item: The National Basic Research Program (973 Program) of China under contract No. 2013CB956203; the National Natural Science Foundation of China under contract No. 41375063; the Junior Fellowships for CAST Advanced Innovation Think-tank Program under contract No. DXB-ZKQN-2016-019.

*Corresponding author, E-mail: zhanglif_qxxy@sina.cn

activity changes. Recently, by using eight different data sets from various sources available for the last 100 a (1910–2009), Yu et al. (2016) (hereafter YEA16) found that the statistically significant ~10 a KE SST variability only becomes apparent after the 1980s, while the KE SST shows another significant variability with a period of ~6 a between 1930 and 1950. In addition, both the two cycles of the KE SST variability were found to be closely related to the AL activity changes but with distinct physical processes: the KE SST variability was primarily triggered by the AL north-south shift through the bridge of Rossby waves with a period of ~10 a between 1980 and 2009, consistent with Sugimoto and Hanawa (2009), but it was strongly impacted by the anomalous surface flux forcing and Ekman heat advection associated with the AL intensity variation with a period of ~6 a between 1930 and 1950. Although YEA16 advanced the understanding of long-term KE SST variability, they did not explain why these different cycles of variability respond to the AL activity over the two timespans. Motivated by this, our present study aims at answering how the AL activity determines the two periods (i.e., ~6 and ~10 a) of the KE SST variability during 1930–1950 and 1980–2009, respectively. It is believable that this current work will deepen the understanding of the generation of dual-period KE SST variability and can be regarded as an extension of the work undertaken by YEA16.

The remainder of the paper is arranged as follows: Section 2 describes data and methods; Section 3 investigates the atmospheric forcing of dual-period KE SST variability; Section 4 examines the relationship between the KE dynamic state fluctuations and the dual-period KE SST variability; Section 5 discusses the potential mechanisms associated with the dual-period KE SST response to AL activity; and concluding remarks are given in Section 6.

2 Data and methodology

2.1 *Reanalysis data*

Two century-long atmospheric and oceanic reanalysis data sets were used. A sea level pressure (SLP) and a surface wind stress were obtained from the ensemble-mean fields of the Twentieth-Century Reanalysis data set version 2 (20CRv2), which contains the synoptic-observation-based estimate of global tropospheric variability at a 6-hourly temporal resolution and 2° spatial resolution (Compo et al., 2011). The SSH was derived from the Simple Ocean Data Assimilation (SODA) reanalysis product with a resolution of 0.5°×0.5° at 40 vertical levels, which was created by assimilating timely temperature and salinity observational profiles based on the Parallel Ocean Program ocean model (Carton and Giese, 2008). Compared with other reanalyses, the 20CRv2 proves to be generally of high quality in assessing the variations in circulations over the extratropical Northern Hemisphere (Compo et al., 2011; Zheng et al., 2017). The SODA can also reasonably capture the year-to-year variability of the Kuroshio Current (Wu et al., 2012). Therefore, these two datasets are believable to investigate the variability of the KE SST and the AL activity and their relationship. In the present study, consistent with YEA16, only the winter season (January–March, hereafter JFM), when the greatest ocean-atmosphere interaction occurs, is considered.

2.2 *Indices*

Several indices used by YEA16 are also used here to depict the KE SST variability and changes in AL activity, namely: (1) the merged KE SST index (MKESSTI), which is defined as the ensemble mean of the SST anomalies averaged over the KE region (32–38°N, 142–180°E) and which uses data from the eight data sets including interpolated reconstructions as well as uninterpolated archives; and (2) the AL indices including the intensity index (INTI) and the north-south shift index (NSSI), which are calculated based on the 20CRv2 data set. The INTI indicates the AL intensity variation and the NSSI represents the AL north-south shift. More details of the data sets and methods used in the calculations of the MKESSTI and AL indices can be found in YEA16.

2.3 *Effective temporal degrees of freedom*

The statistical significance of all regression or correlation coefficients between two time series in this study is assessed by taking the serial autocorrelation into consideration, which reduces the number of effective temporal degrees of freedom. For the regression or correlation between the JFM mean data of two variables X and Y, the effective sample size N^* is estimated using the modified Chelton method (Pyper and Peterman, 1998; Ding et al., 2015). The value of the effective sample size can be derived from the following theoretical approximation:

$$N^* \approx \frac{N}{1+2\sum_{i=1}^{N}\frac{N-i}{N}\rho_X(i)\rho_Y(i)}, \tag{1}$$

where N is the sample size, and $\rho_X(i)$ and $\rho_Y(i)$ are the autocorrelations of the two sampled time series X and Y, respectively.

3 Atmospheric forcing of the dual-period KE SST variability

To further verify that the atmospheric forcing of the dual-period KE SST variability is linked to the AL activity, we calculated the regressions of the SLP and wind stress fields upon the normalized MKESSTI using specific lead times based on ~6 and ~10 a first-order Butterworth band-pass-filtered anomalies. Lead times of 3 and 5 a (i.e., half of the ~6 and ~10 a cycles of variability, respectively) are selected to obtain the forcing processes associated with the two cycles of the KE SST variability.

For the ~6 a cycle between 1930 and 1950, at a lead time of 3 a, a basin scale negative SLP anomaly and the accompanying cyclone dominate almost the entire North Pacific (Fig. 1a), indicating a strengthened AL. After that (at a lead time of 2 a), these anomalies weaked and shift southeastwards. Meanwhile, the positive SLP anomalies (anticyclones) appear over the KE region, the central subtropical Pacific, the northeastern Pacific, and North American continent (Fig. 1b). These SLP and wind stress anomalies develop and merge to become a basin scale anomaly two years later (Figs 1c and d), which correspond to a weakened AL. These results indicate that the AL intensity has a positive relationship with the KE SST three years later and a negative relationship with the KE SST simultaneously. The simultaneous KE SST-AL relationship was also reported by YEA16, who revealed that the AL intensity variation impacts the simultaneous KE SST via anomalous surface heat flux and Ekman heat transport. However, the lagged KE SST-AL relationship has not been reported in previous studies, which suggests that there is another impact of the AL on the KE SST. This is important for the formation of the ~6 a KE SST variability and will be investigated in the following section.

For the ~10 a cycle between 1980 and 2009, at a lead time of 5 a, the KE SST-related SLP and wind stress anomalies are generally characterized by an insignificant north-south dipole with the positive SLP anomaly (anticyclone) centered over the Bering Sea and the negative SLP anomaly (cyclone) covering most parts of

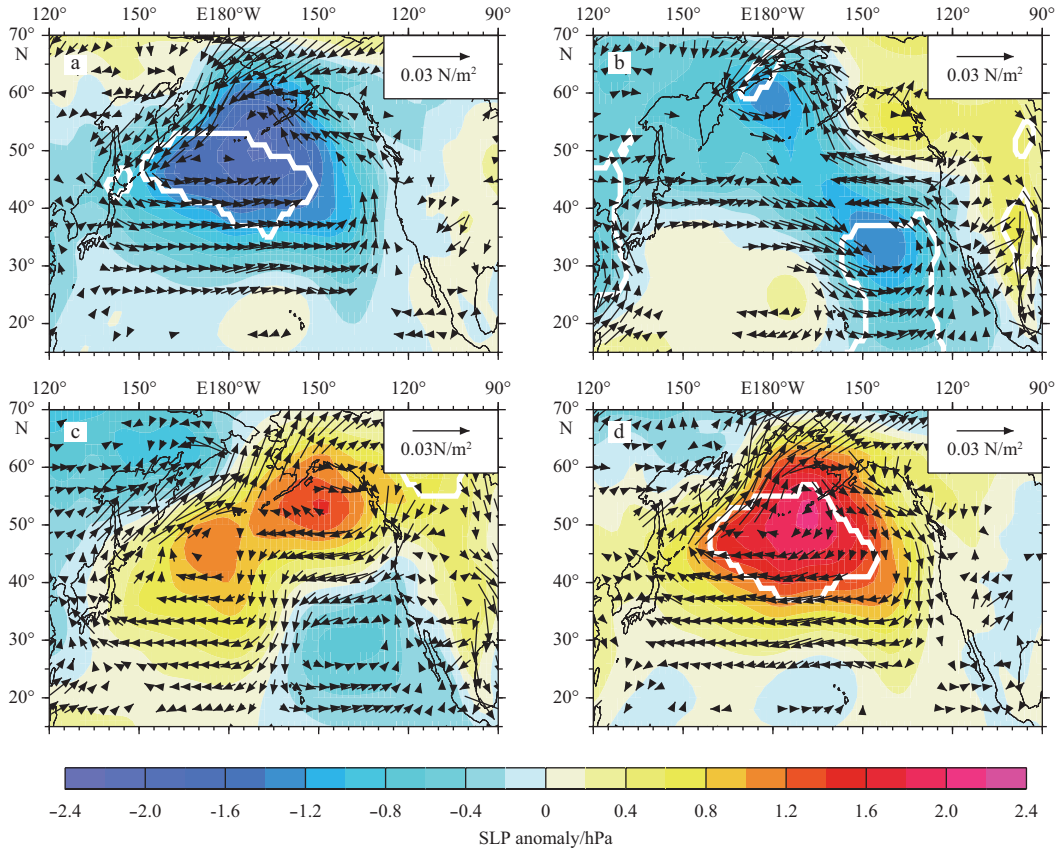

Fig. 1. Regressions of the SLP (shading) and wind stress (vectors) fields upon the normalized MKESSTI based on the ~6 a band-pass-filtered anomalies during 1930–1950 using lead time of 3 a (a), 2 a (b), 1 a (c), and 0 a (d). The white contours imposed on the SLP shading denote the 90% confidence level. Only the wind stress vectors exceeding the 90% confidence level are plotted.

the mid-latitude North Pacific (Fig. 2a). This pattern is similar to the negative phase of the North Pacific Oscillation (NPO) (Wallace and Gutzler, 1981; Linkin and Nigam, 2008), which indicates the AL is located more southward than normal (Sugimoto and Hanawa, 2009). Therefore, the AL latitudinal position has a negative relationship with the KE SST five years later. Moreover, the pattern of NPO-like dipole here also bears some similarity to the atmospheric component of eastern North Pacific mode (ENPM) with anomaly occurring in the vicinity of the Aleutian Islands, and anomaly of the opposite polarity over northwestern Canada (Wu and Liu, 2003). However, as this NPO-like dipole is not significant, the negative lagged KE SST-AL relationship is weak. From lead time of 3–4 a, the positive SLP anomaly (anticyclone) located in the Bering Sea decays, disappears, and is replaced mainly by the negative SLP anomaly (cyclone) migrating from the south. At the same time, the positive SLP anomaly (anticyclone) in the eastern North Pacific merges with that newly appearing in the western North Pacific (Figs 2b and c), and a positive NPO-like dipole forms, associated with the northward shift of the AL. Subsequently, the dipole structure continues to develop and becomes pronounced for lead time of 1–2 a (Figs 2d and e), but weakens at a lead time of 0 a (Fig. 2f), indicating the strong connection between the AL latitudinal position and the KE SST 1–2 a later. This lagged relationship between the AL latitudinal position and the KE SST was also found by YEA16, and they showed that the AL north-south shift affects the KE SST two years later through oceanic Rossby waves. However, it is worth noting that a dipole structure SLP at a lead time of 5 a requires an additional 2–3 a to evolve into a significant dipole with an opposite sign, indicating the AL northward shift. These delays have been overlooked previously, but are indispensable for the formation of the ~10 a cycle of the KE SST variability, which is highlighted in the present study. According to above results, strong lagged relationship between the AL activity and the KE SST appears on both the time scales of ~6 and ~10 a, verifying the significant forcing of AL activity on the dual-period KE SST variability.

4 Relationship between KE dynamic state fluctuations and dual-period KE SST variability

As reviewed in introduction, the SST variability in the KE region is modulated mainly by fluctuations in its dynamic state. Specifically, when the KE jet intensifies and shifts northward in its stable state, a warm KE SST anomaly tends to occur, and vice versa (Qiu, 2000; Vivier et al., 2002). Therefore, the dual-period KE SST variability is supposed to be related to changes in the KE jet strength and latitudinal position. In order to quantitatively depict KE jet intensity variation and meridional shift, we use the SODA SSH data to derive the geostrophic current velocity $|V_g|$ as follows:

$$|V_g|^2 = \left(\frac{g}{f}\frac{\partial h}{\partial x}\right)^2 + \left(\frac{g}{f}\frac{\partial h}{\partial y}\right)^2, \quad (3)$$

where h is the SSH, g is the gravity constant, and f is the Coriolis parameter. We then calculate the maximum velocity and its latitude at each longitude within the KE meridional band (32°–38°N),

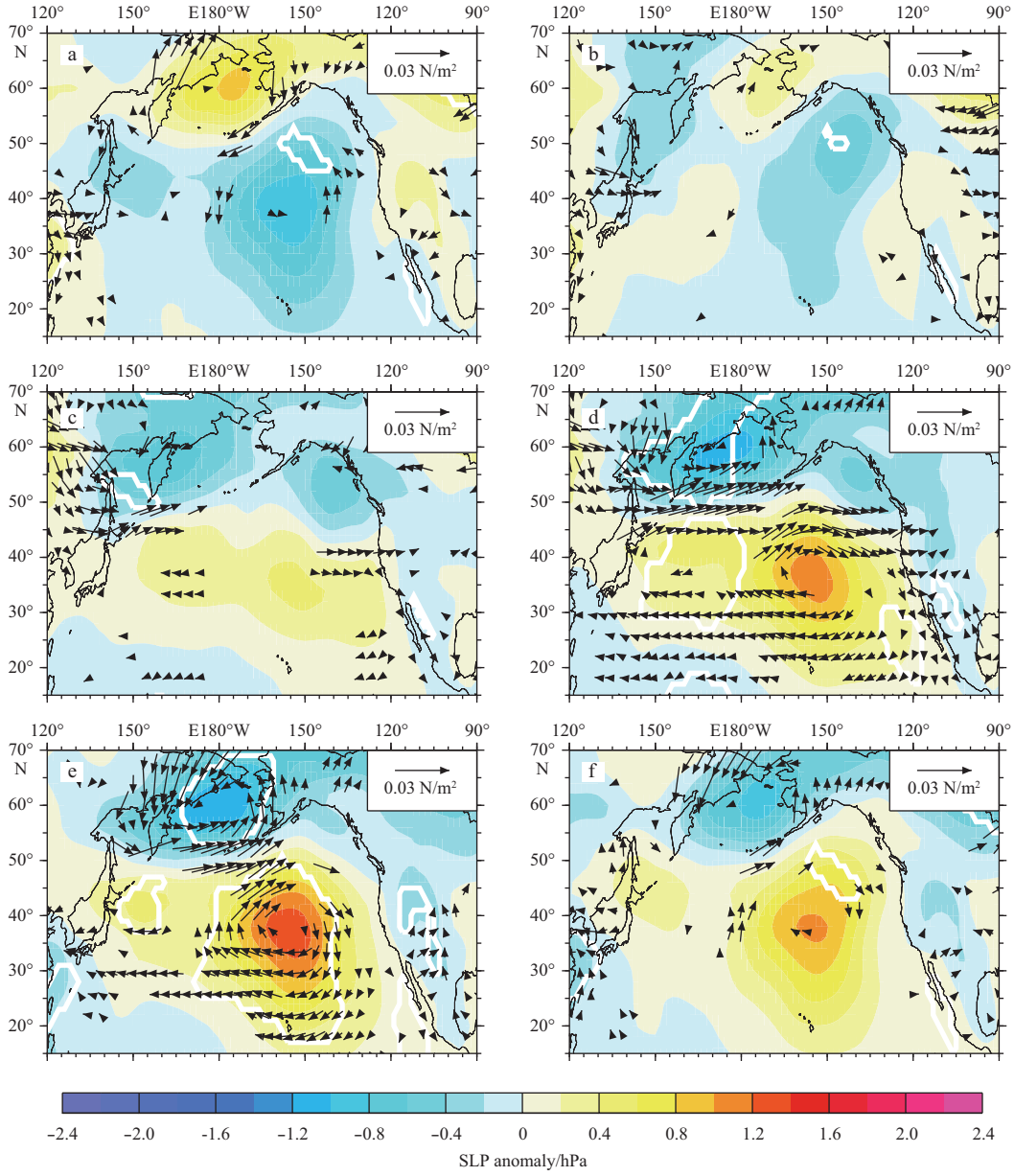

Fig. 2. As for Fig. 1, but for the ~10 a band-pass-filtered anomalies during 1980–2009 at lead time of 5 a (a), 4 a (b), 3 a (c), 2 a (d), 1 a (e), and 0 a (f).

and define their average values between 142° and 180°E as the KE jet strength and latitudinal position, as in Taguchi et al. (2007) and Kelly et al. (2010).

Figure 3 shows the normalized MKESSTI time series, as well as the KE jet strength and latitudinal position, smoothed using windows of 6 and 10 a. For the ~6 a cycle (Fig. 3a), both the MKESSTI and KE jet strength time series have large amplitudes, and they also show a high simultaneous correlation (r=0.83) between 1930 and 1950, which exceeds the 90% confidence level. However, the KE jet latitudinal position time series has a relatively small amplitude, and it is almost uncorrelated with the MKESSTI (r=–0.09) and with the KE jet strength time series (r=0.00) simultaneously between 1930 and 1950. The situation is exactly the reverse of the longer ~10 a cycle between 1980 and 2009 (Fig. 3b). The amplitudes of both the MKESSTI and KE jet latitudinal position time series are large and their simultaneous correlation is also significantly high (r=0.97). Although the KE jet strength time series has comparable amplitudes, it shows little correlation with the MKESSTI (r=0.01) or with the KE jet latitudinal position time series (r=0.19) simultaneously. These results indicate that the KE jet strength change (meridional shift) can be taken as a proxy of the ~6 (~10) a KE SST variability between 1930 and 1950 (1980 and 2009).

5 Mechanisms associated with the dual-period KE SST response to the AL activity

From the above analysis, the KE jet intensity variation and meridional shift are closely related to the ~6 and ~10 a KE SST variability, respectively. In addition, previous studies indicate that these two KE dynamic state fluctuations are also significantly impacted by the wind-induced Rossby waves associated with the AL activity changes (e.g., Qiu, 2003; Qiu and Chen, 2005, 2010; Kwon and Deser, 2007; Qiu et al., 2014; Seo et al., 2014). Therefore, it is reasonable to speculate that the AL activity can

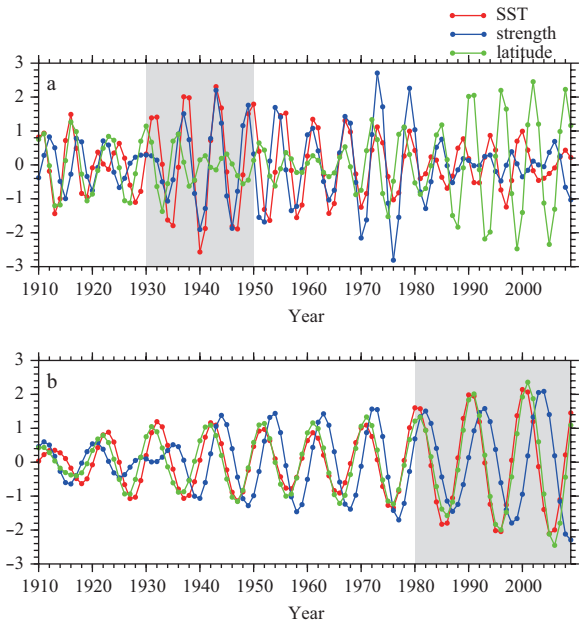

Fig. 3. Normalized time series of the ~6 a band-pass-filtered MKESSTI (red line), KE jet strength (blue line), and latitude (green line) after removal of the linear trend (a). As for Fig. 3a, but for the 10 a band-pass-filtered time series (b). Gray shading indicates the two key time periods: 1930–1950 and 1980–2009.

impact the dual-period KE SST variability by affecting the KE jet intensity variation and meridional shift via the bridge of oceanic Rossby waves. This section investigates how the AL activity induces the dual-period KE SST response at different timespans over the past century. First, we explore the impacts of oceanic Rossby waves on the KE dynamic state fluctuations associated with the dual-period KE SST variability, and then discuss how the AL activity excites these Rossby waves.

5.1 *Impacts of oceanic Rossby waves*

Here, as in YEA16, we use the annual-mean SSH anomalies to detect the Rossby waves, which are smoothed using a Gaussian spatial filter with an *e*-folding scale of 200 km, to highlight the large-scale variations. Figure 4a shows a lag-longitude correlation diagram of the KE jet strength time series with the SSH anomalies averaged within the meridional band of 33°–35°N, where the zonal mean KE axis is located (Seo et al., 2014), on the time scale of ~6 a during 1930–1950. Although the change in the KE jet strength shows significant positive correlations with the SSH anomalies over the KE region, the latter is not caused by Rossby waves that originate in the central North Pacific (160°E–160°W), as negative correlations are shown therein when the change in the KE jet strength lags by 2–3 a. This indicates that the change in the KE jet strength is not modulated by the Rossby waves that originate in the central North Pacific. In contrast, on the time scale of ~10 a during 1980–2009, the meridional shift in the KE jet is significantly correlated with the SSH anomalies over the KE region, which are formed around 180°–170°W and propagate westwards into the KE region 2–3 a later (Fig. 4b), indicating that the meridional shift in the KE jet is initiated by the Rossby waves that originate in the central North Pacific.

Even though the ~10 a meridional shift in the KE jet during 1980–2009 can be explained by Rossby wave dynamics, the factors driving the ~6 a cycle of change in the KE strength during 1930–1950 remain to be determined. To investigate this topic, we calculate the regressions of the geostrophic current velocity upon the normalized KE jet strength time series for lead time of 3 to 0 a based on the ~6 a band-pass filtered anomalies during this timespan (Fig. 5). At a lead time of 3 a, there are significant negative velocity anomalies around the mean position of the KE axis where the maximum climatological velocity is located (Fig. 5a), featuring a weakened KE jet. For leads of 1 to 2 a, positive velocity anomalies appear and become significant around the mean position of the Kuroshio to the east of Taiwan (KET) (Figs 5b and c). Subsequently, the KE jet is significantly intensified at a lead time

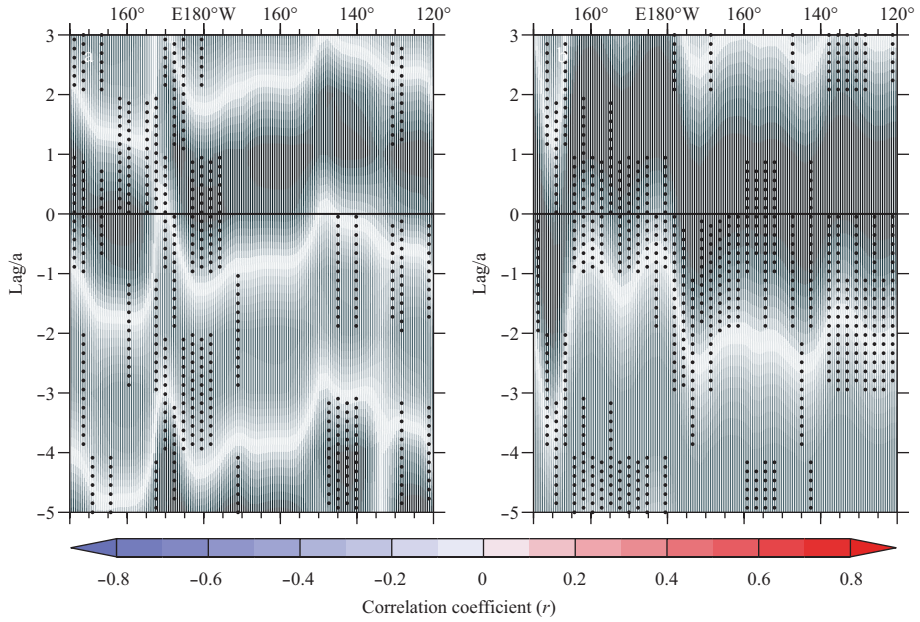

Fig. 4. Lag-longitude correlation diagram of the KE jet strength time series with the SSH anomalies averaged within the meridional band of 33°–35°N on the time scale of ~6 a during 1930–1950. Positive lags indicate that the KE jet strength time-series has lead lags. The stippled areas indicate where significance exceeds the 90% confidence level (a). As for Fig. 4a, but for the KE jet latitudinal position time series and SSH anomalies on the time scale of ~10 a during 1980–2009 (b).

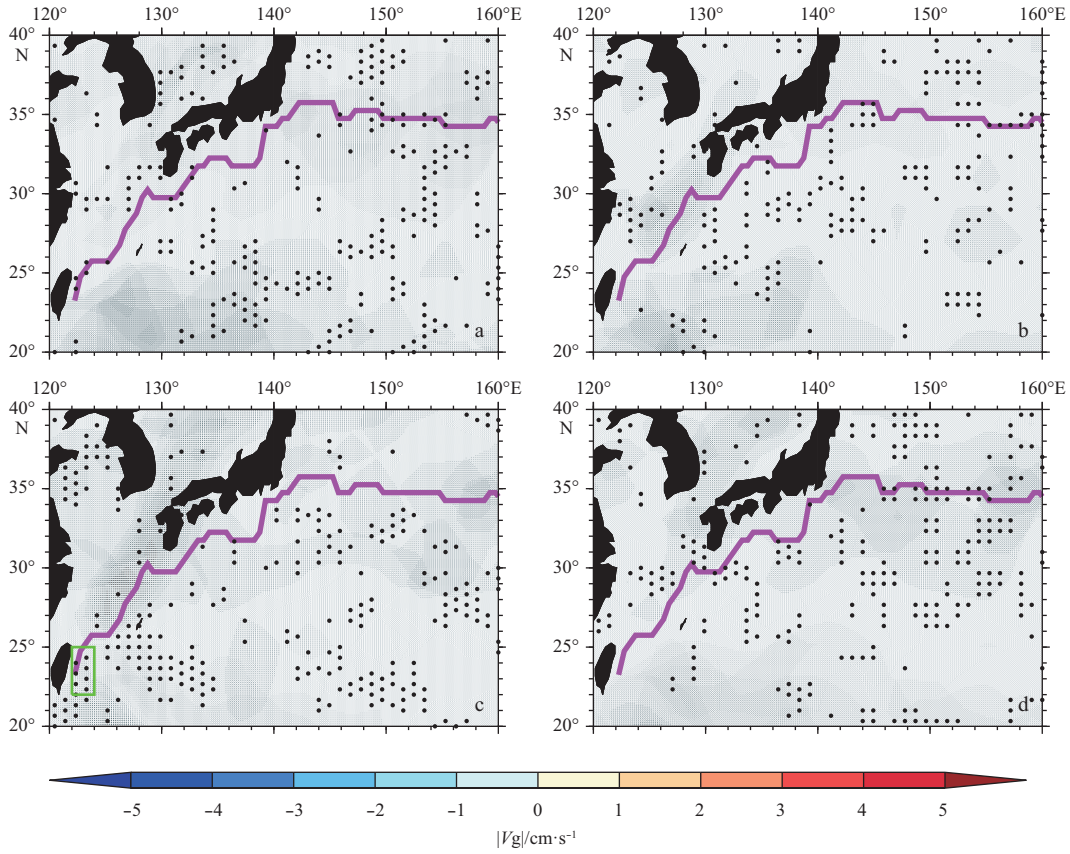

Fig. 5. Regressions of the geostrophic current velocity upon the normalized KE jet strength time-series based on the ~6 a band-pass filtered anomalies during the period 1930–1950 for lead times of 3 a (a), 2 a (b), 1 a (c), and 0 a (d). The stippled areas indicate the significance exceeds the 90% confidence level. The purple line in the four panels indicates the mean position of the Kuroshio Current and its extension, where the maximum climatological velocity is located. The green rectangle in Fig. 5c represents the area referred to here as east of Taiwan (22°–25°N, 122°–124°E).

of 0 a (Fig. 5d). These results indicate that the velocity anomalies around the KET may be closely related to the change in the KE jet strength one year later. To validate this finding, we calculated the geostrophic velocity anomalies averaged over the east of Taiwan (22°–25°N, 122°–124°E). Indeed, for the ~6 a periodicity between 1930 and 1950, the correlation between the KET velocity anomalies and the KE jet strength change reaches its maximum value (r=0.93) when the KET velocity anomalies lead by 1 a, and this is consistent with the results shown in Fig. 5. The lagged relationship between the KET velocity anomalies and the KE jet strength change can be explained by the advection of the geostrophic velocity anomalies (V_g') by the mean velocity of KET ($\overline{V}$), that is $\overline{V}\nabla V_g'$. By using a simple advection-diffusion numerical model, Park et al. (2012) have found that only the mean Kuroshio current in the southern flank of the East China Sea (near the KET) is strong enough to transport the local SST anomalies to the downstream KE region one year later. This discovery supports the notion that the mean advection via the mean KET current of geostrophic velocity anomalies can cause the significant velocity anomalies over the KE region lagged by 1 a and eventually results in a strengthened (weakened) KE jet. After the KE jet intensifies (weakens), the resulted anomalous geostrophic advection tends to warm (cool) the KE SST (Qiu, 2000). These results indicate that the KET velocity anomalies are closely related to the KE jet intensity variation and thus the KE SST one year later on the time scale of ~6 a during 1930–1950.

Next, whether the ~6 a KET velocity anomalies are impacted by the oceanic Rossby waves is investigated. Figure 6a shows a longitude-time diagram of the ~6 a band-pass-filtered SSH anomalies averaged within the KET meridional band (22°–25°N) during 1930–1950. It is evident that there are Rossby waves reaching the east of Taiwan, and these oceanic waves may have modulated the KET velocity variation. As shown in Fig. 6b, the KET velocity anomalies are closely correlated with the SSH anomalies over the east of Taiwan, which form around 180°E–160°W and propagate westwards to the east of Taiwan two years later, confirming that the KET velocity anomalies are forced by the Rossby waves that originate in the central subtropical Pacific (160°E–160°W) on the time scale of ~6 a during 1930–1950. Therefore, it is inferred that the Rossby waves that originate in the central subtropical Pacific can influence the ~6 a KE jet strength change via the bridge of the KET velocity anomalies and thus affect the ~6 a KE SST variability. Furthermore, these Rossby waves are most evident during 1930–1950 (not shown), which may explain why the significant ~6 a KE SST variability is found only during this timespan (see Fig. 2 in YEA16).

5.2 *Excitation of Rossby waves by AL activity*

According to the above analysis, the KE dynamic state fluctuations associated with the dual-period KE SST variability are caused by the Rossby waves that originate in the central subtropical Pacific and central North Pacific. These oceanic signals may

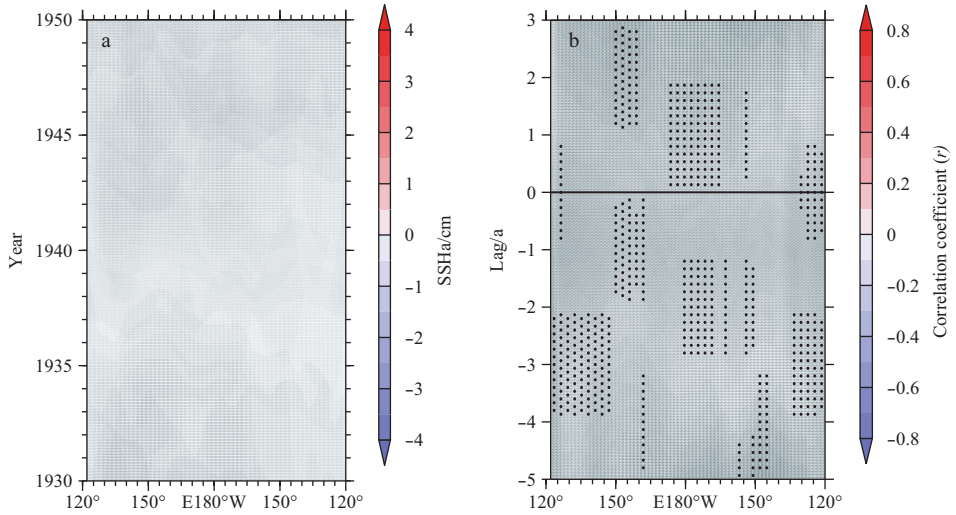

Fig. 6. Hovmöller diagram of the 6 a band-pass-filtered annual mean SSH anomalies averaged within the KET latitudinal band (22°–25°N) during 1930–1950 (a), and the lag-longitude correlation diagram of the 6 a band-pass-filtered KET velocity time series with the SSH anomalies in Fig. 6a. Positive lags mean that the KET intensity has lead lags. The stippled areas indicate statistical significance exceeding the 90% confidence level (b).

be an important way by which the AL activity impacts the KE SST-related dynamic state fluctuations on time scales of ~6 and ~10 a. To verify this possibility, we investigate the atmospheric forcing of the aforementioned Rossby waves. Figure 7a shows the regressions of the wind stress curl (WSC) field upon the normalized KET velocity time series at a lag of 2 a on the time scale of ~6 a during 1930–1950. Similar results can also be derived from the regressions upon the normalized KE jet strength time series at a lag of 3 a (not shown). We find that along the KET meridional band, there are significant negative WSC anomalies in the central subtropical Pacific that generate positive SSH anomalies through Ekman convergence. A visual inspection reveals that this regression pattern is spatially similar to that associated with the AL intensity variation (see Fig. 10b in YEA16), which is supported by a high positive correlation (r=0.96) between the INTI and the KET velocity time series at a lag of 2 a. The simultaneous correlations (r>0.64) between the INTI and the SSH anomalies in the central subtropical Pacific are generally high, and their maximum value is 0.96 at 180°. These results indicate that the AL intensity variation can excite the Rossby waves that originate in the central subtropical Pacific, which are associated with the ~6 a cycle in the KE strength change, thus impacting the ~6 a KE SST variability.

Similar to Fig. 7a, Fig. 7b shows the regression pattern of the WSC field upon the normalized KE jet latitudinal position time series at a lag of 2 a on the time scale of ~10 a during 1980–2009. An almost identical pattern is obtained from the regressions upon the normalized KE jet latitudinal position time series at a lag of 3 a (not shown). Significant negative WSC anomalies are found in the central North Pacific along the meridional band of 33°–35°N, which can induce positive SSH anomalies through Ekman convergence. This regression pattern closely resembles that

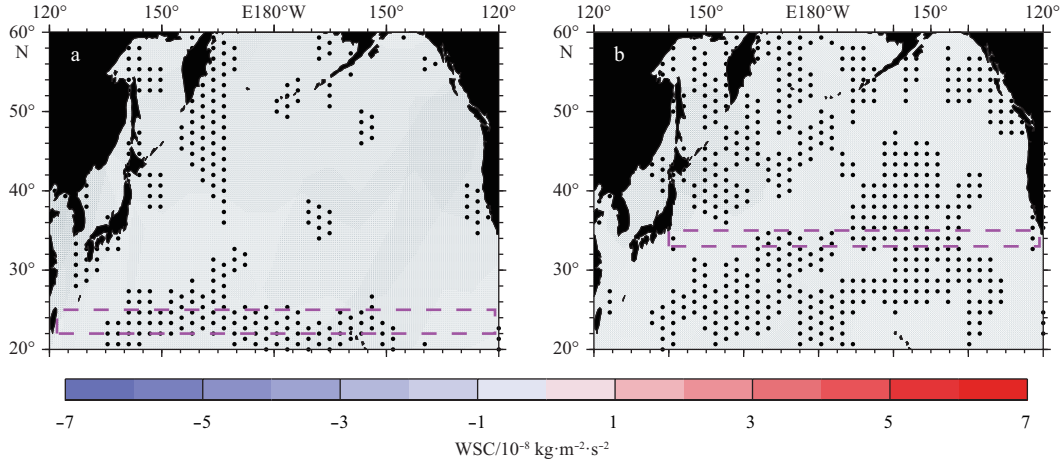

Fig. 7. Regressions of the wind stress curl (WSC) field upon the normalized KET velocity time series at a lag of 2 a based on the ~6 a band-pass-filtered anomalies during 1930–1950. The stippled areas indicate statistical significance exceeding the 90% confidence level (a). As for Fig. 7a, but for the normalized KE jet latitudinal position time series at a lag of 2 a based on the ~10 a band-pass-filtered anomalies during 1980–2009 (b). The dashed purple rectangles in Figs 7a and b represent the meridional bands of 22°–25°N and 33°–35°N, respectively.

upon the NSSI (see Fig. 10a in YEA16). Indeed, the correlation (r=0.97) between the NSSI and the KE jet latitudinal time series at a lag of 2 a is positive and high. YEA16 revealed that the NSSI is, simultaneously, highly correlated with the SSH anomalies in the central North Pacific. Accordingly, the Rossby waves that originate in the central North Pacific, which drive the ~10 a cycle of meridional shift in the KE jet, are excited by the AL north-south shift, as was also proposed by Qiu et al. (2014) and Seo et al. (2014). Through this process, the AL north-south shift has an influence on the ~10 a KE SST variability.

As demonstrated above, Rossby waves generated by the AL intensity variation and north-south shift are essential for initiating the KE SST variability with periods of ~6 and ~10 a, respectively. The basin-crossing time of these Rossby waves, together with some additional delays, generate the two periodicities. For the ~6 a cycle, there is a 2 a delay between the AL intensity variation and the KET velocity anomalies via the Rossby waves that originate in the central subtropical Pacific. An additional 1 a delay is found between the KET velocity anomalies and the KE jet strength change and KE SST anomaly. The sum of these delays induces a half cycle of ~6 a. On the other hand, for the ~10 a cycle, the Rossby waves induced by the AL north-south shift originate in the central North Pacific, and take 2–3 a to reach the KE region with a lower speed than that in the subtropics (Chelton and Schlax, 1996). However, it is worth noting that the NPO-like dipole requires an additional 2–3 a to evolve into a dipole with the opposite sign, and this process corresponds to the AL northward or southward shift, enabling the excitation of the Rossby waves. The total delays result in a half cycle of ~10 a.

The previous analyses cover the forcing of the dual-period KE SST variability by the AL activity. To establish the closed cycles of ~6 and ~10 a, we also investigate the AL response patterns to the dual-period KE SST anomaly by calculating the regressions of the SLP and wind stress fields upon the MKESSTI with a lead time of 1 a or longer (not shown). These patterns exhibit similar spatial structures and evolutions to those in Figs 1 and 2, but with opposite signs, indicating that the feedbacks of the KE SST anomaly on the AL forcing are both negative for periodicities of ~6 and ~10 a. These feedbacks are possibly caused by the profound impacts of the KE SST anomaly on the overlying storm tracks (Kushnir et al., 2002; Nakamura et al., 2004; Bengtsson et al., 2006). Therefore, the dual-period KE SST variability can be generated by the two-way KE SST-AL coupling. However, it is noteworthy that an asymmetry may be existed in the atmospheric response to dual-period KE SST anomaly. Révelard et al. (2016) have found that the atmospheric response primarily occurs during the KE warming, while there is little large-scale response during the cooling. And they proposed this asymmetry is due to the difference between the impacts of the KE warming and cooling on the overlying storm tracks. Accordingly, the AL response to the KE cooling may be too weak to loop the KE SST-AL coupled variability for periodicities of ~6 and ~10 a compared with the warming. This reflects the complexity of mid-latitude ocean-atmosphere interaction. Thus, future studies using fully coupled climate models is clearly needed to further validate whether the dual-period KE variability is the manifestation of KE SST-AL coupling and investigate its underlying mechanisms.

6 Concluding remarks

In this study, we investigate how the AL activity induces the dual-period KE SST variability during the two timespans identified by YEA16. On the time scale of ~6 a during 1930–1950, negative WSC anomalies associated with an intensified AL are evident in the central subtropical Pacific, and these anomalies generate the positive SSH anomalies through Ekman convergence. When these wind-induced SSH anomalies propagate westward to the east of Taiwan as Rossby waves with a 2 a lag, the positive velocity anomalies appear around the KET and then the mean advec-

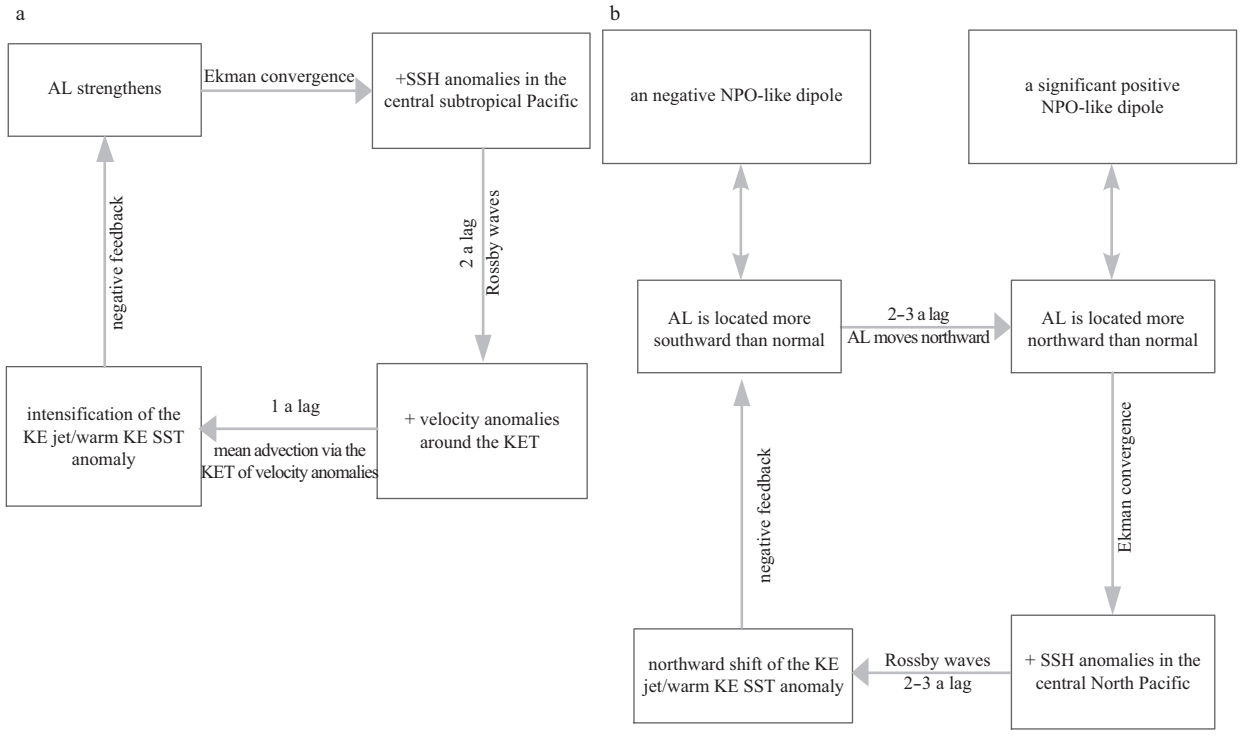

Fig. 8. Schematic representation of the two-way coupled relationship between KE SST and AL activity for the periodicities of ~6 a during 1930–1950 (a) and ~10 a during 1980–2009 (b).

tion via the KET of velocity anomalies leads to a strengthened KE jet and thus an increase in KE SST one year later.

On the time scale of ~10 a during 1980–2009, an negative NPO-like dipole, which indicates the AL is located more southward than normal, takes 2–3 a to develop into a significant positive NPO-like dipole, and this process corresponds to the northward shift of the AL. This AL activity leads to large negative WSC signals in the central North Pacific, which are able to induce the positive SSH anomalies through Ekman convergence. These oceanic signals then propagate westward into the KE region after 2–3 a, favoring a northward shift of the KE jet, thus leading to the warming of KE SST.

The AL response patterns to this dual-period KE SST variability exhibit similar spatial structures and evolution to the forcing patterns, but with the opposite signs. This indicates that the feedbacks of the KE SST anomaly on the AL forcing are both negative for periodicities of ~6 and ~10 a. Therefore, the dual-period KE SST variability can be generated by the two-way KE-SST-AL coupling. The associated process is summarized in Fig. 8; however, the results discussed in this paper should be further verified and analyzed by using fully coupled climate models.

References

Bengtsson L, Hodges K I, Roeckner E. 2006. Storm tracks and climate change. J Climate, 19(15): 3518–3543

Carton J A, Giese B. 2008. A reanalysis of ocean climate using Simple Ocean Data Assimilation (SODA). Mon Wea Rev, 136(8): 2999–3017

Chelton D B, Schlax M G. 1996. Global observations of oceanic Rossby waves. Science, 272(5259): 234–238

Compo G P, Whitaker J S, Sardeshmukh P D, et al. 2011. The twentieth century reanalysis project. Quart J Roy Meteor Soc, 137(654): 1–28, doi: 10.1002/qj.776

Ding Ruiqiang, Li Jianping, Tseng Y H. 2015. The impact of South Pacific extratropical forcing on ENSO and comparisons with the North Pacific. Climate Dyn, 44(7-8): 2017–2034

Frankignoul C, Sennéchael N. 2007. Observed influence of North Pacific SST anomalies on the atmospheric circulation. J Climate, 20(3): 592–606

Ishi Y, Hanawa K. 2005. Large-scale variabilities of wintertime wind stress curl field in the North Pacific and their relation to atmospheric teleconnection patterns. Geophys Res Lett, 32(10): L10607, doi: 10.1029/2004GL022330

Kelly K A, Small R J, Samelson R M, et al. 2010. Western boundary currents and frontal air-sea interaction: Gulf Stream and Kuroshio Extension. J Climate, 23(21): 5644–5667

Kushnir Y W, Robinson W A, Bladé I, et al. 2002. Atmospheric GCM response to extratropical SST anomalies: synthesis and evaluation. J Climate, 15(16): 2233–2256

Kwon Y O, Deser C. 2007. North Pacific decadal variability in the Community Climate System Model version 2. J Climate, 20(11): 2416–2433

Linkin M E, Nigam S. 2008. The North Pacific Oscillation-west Pacific teleconnection pattern: mature-phase structure and winter impacts. J Climate, 21(9): 1979–1997

Liu Zhengyu, Liu Yun, Wu Lixin, et al. 2007. Seasonal and long-term atmospheric responses to reemerging North Pacific Ocean variability: a combined dynamical and statistical assessment. J Climate, 20(6): 955–980

Nakamura H, Sampe T, Tanimoto Y, et al. 2004. Observed associations among storm tracks, jet streams and midlatitude oceanic fronts. In: Wang C, Xie S P, Carton J A, eds. Earth's Climate: The Ocean-Atmosphere Interaction. Washington: American Geophysical Union, 329–346

Park Y H, Yoon J H, Youn Y H, et al. 2012. Recent warming in the western North Pacific in relation to rapid changes in the atmospheric circulation of the Siberian High and Aleutian Low systems. J Climate, 25(10): 3476–3493

Pyper B J, Peterman R M. 1998. Comparison of methods to account for autocorrelation in correlation analyses of fish data. Can J Fish Aquat Sci, 55(9): 2127–2140

Qiu Bo. 2000. Interannual variability of the Kuroshio extension system and its impact on the wintertime SST field. J Phys Oceanogr, 30(6): 1486–1502

Qiu Bo. 2003. Kuroshio Extension variability and forcing of the Pacific decadal oscillations: Responses and potential feedback. J Phys Oceanogr, 33(12): 2465–2482

Qiu Bo, Chen Shuiming. 2005. Variability of the Kuroshio Extension jet, recirculation gyre, and mesoscale eddies on decadal time scales. J Phys Oceanogr, 35(11): 2090–2103

Qiu Bo, Chen Shuiming. 2010. Eddy-mean flow interaction in the decadally modulating Kuroshio Extension system. Deep-Sea Res: II, 57(13-14): 1098–1110

Qiu Bo, Chen Shuiming, Schneider N, et al. 2014. A coupled decadal prediction of the dynamic state of the Kuroshio Extension system. J Climate, 27(4): 1751–1764

Qiu Bo, Schneider N, Chen Shuiming. 2007. Coupled decadal variability in the North Pacific: an observationally constrained idealized model. J Climate, 20(14): 3602–3620

Révelard A, Frankignoul C, Sennéchael N, et al. 2016. Influence of the decadal variability of the Kuroshio Extension on the atmospheric circulation in the cold season. J Climate, 29(6): 2123–2144

Seager R, Kushnir Y, Naik N H, et al. 2001. Wind-driven shifts in the latitude of the Kuroshio-Oyashio Extension and generation of SST anomalies on decadal timescales. J Climate, 14(22): 4249–4265

Seo Y, Sugimoto S, Hanawa K. 2014. Long-term variations of the Kuroshio Extension path in winter: meridional movement and path state change. J Climate, 27(15): 5929–5940

Sugimoto S, Hanawa K. 2009. Decadal and interdecadal variations of the Aleutian low activity and their relation to upper oceanic variations over the North Pacific. J Meteor Soc Japan, 87(4): 601–614

Sugimoto S, Hanawa K. 2011. Roles of SST anomalies on the wintertime turbulent heat fluxes in the Kuroshio-Oyashio confluence region: influences of warm eddies detached from the Kuroshio Extension. J Climate, 24(24): 6551–6561

Taguchi B, Xie Shangping, Schneider N, et al. 2007. Decadal variability of the Kuroshio Extension: observations and an eddy-resolving model hindcast. J Climate, 20(11): 2357–2377

Tanimoto Y, Nakamura H, Kagimoto T, et al. 2003. An active role of extratropical sea surface temperature anomalies in determining anomalous turbulent heat flux. J Geophys Res, 108(C10): 3304, doi: 10.1029/2002JC001750

Vivier F, Kelly E A, Thompson L A. 2002. Heat budget in the Kuroshio Extension region: 1993-99. J Phys Oceanogr, 32(12): 3436–3454

Wallace J M, Gutzler D S. 1981. Teleconnections in the geopotential height field during the Northern Hemisphere winter. Mon Wea Rev, 109(4): 784–812

Wang Xiaodan, Zhong Zhong, Liu Jianwen, et al. 2012. Propagation characteristic of atmospheric responses to abnormal warm SST in the Kuroshio Extension in winter. Theor Appl Climatol, 108(1-2): 283–292

Wang Xiaodan, Zhong Zhong, Tan Yanke, et al. 2011. Numerical experiment on the effect of the warmer SST in the Kuroshio Extension in winter on the East Asian summer monsoon. J Trop Meteor (in Chinese), 27(4): 569–576

Wu Lixin, Cai Wenju, Zhang Liping, et al. 2012. Enhanced warming over the global subtropical western boundary currents. Nat Climate Change, 2(3): 161–166

Wu Lixin, Liu Zhengyu. 2003. Decadal variability in the North Pacific: The eastern North Pacific mode. J Climate, 16(19): 3111–3131

Yu Peilong, Zhang Lifeng, Zhang Yongchui, et al. 2016. Interdecadal change of winter SST variability in the Kuroshio Extension region and its linkage with Aleutian atmospheric low pressure system. Acta Oceanologica Sinica, 35(5): 24–37

Zheng Chongwei, Wang Qing, Li Chongyin. 2016. An overview of medium- to long-term predictions of global wave energy resources. Renewable and Sustainable Energy Reviews, : doi: 10.1016/j.rser.2017.05.109